Chapter 4 Tryptophan based Polyurethane a Theranostic approach for Tumor killing and *in-vivo* toxicity study to check Localized treatment efficacy

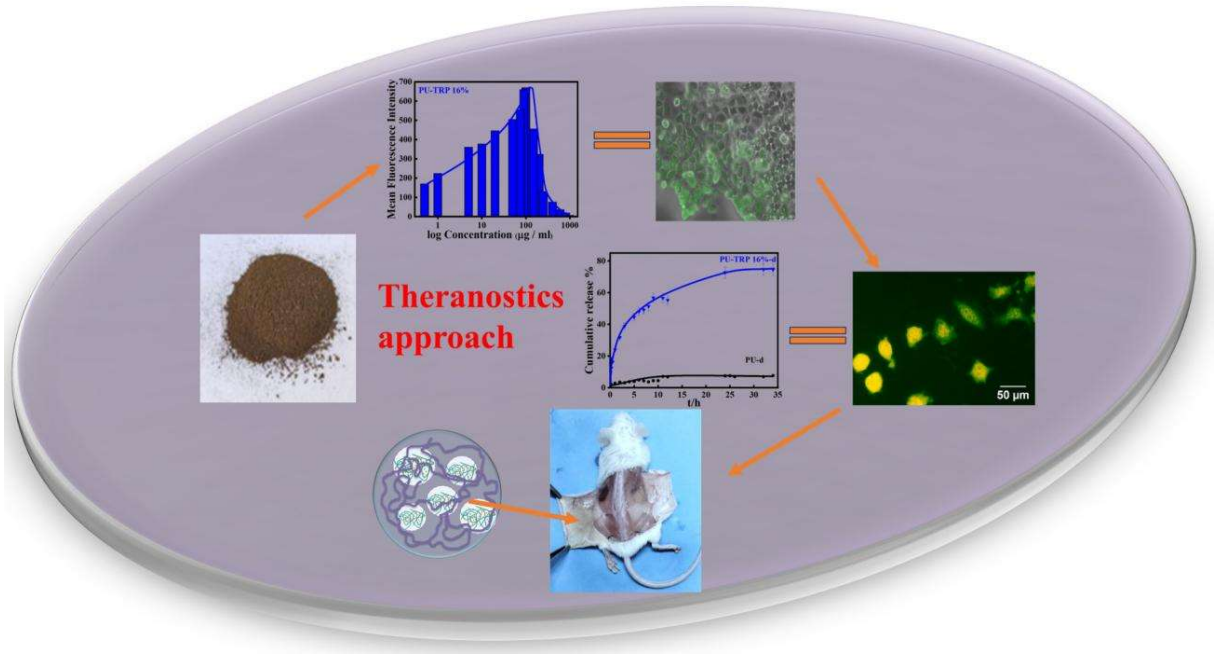

Chapter 4

4.1 Introduction

The theranostics approach[61] in targeted cancer treatment represents a promising advancement in the precision medicine era. The theranostics approach in cancer treatment refers to the integration of both therapy and diagnostics into a single platform, enabling a more personalized and efficient treatment strategy. In the realm of targeted cancer treatment, this approach is particularly valuable because it allows for the simultaneous diagnosis, monitoring, and treatment of the disease using drug delivery systems (DDS). As in chapter 3 we have already established the fact that aliphatic polyurethanes are more biocompatible and have better drug release rates compared to aromatic ones. So, in this chapter, we have modified aromatic (it will provide extended conjugation), PTMG, and 2,4-TDI-based PU with hard segment, amino acid (TRP) for better drug release and biocompatibility. Along with TRP's intrinsic fluorescence properties were exploited for establishing a better DDS. The spectroscopic characterization and the biological response are discussed in a detailed manner in section 4.2.

4.2 Results and Discussion

4.2.1 Spectroscopic Characterization

The synthesis of amino-acid based PU entails a precise regulation of chemical reactions between the hard & soft segments. This controlled reaction leads to the formation of branched structures, as verified by ^{1}H NMR and supported by FTIR and UV-VIS spectroscopy, as illustrated in **Figure 4.2.1a**, **b**, and **c** respectively. The spectra of pure PU display the characteristic peaks at 4.87 and 1.5 ppm {t, $–CH_2–O$, urethane unit}, which shift

to 4.78{t} and 1.47 and other methylene groups at 1.22 ppm for PU- TRP 16%[169–171]. The peaks around 10.22 & 10.88 (s) are attributed to the indole H-bonded and non-bonded -NH- protons, indicating a mixture of two different types of PU[172]. In one type, both, and in other types, only primary NH_2 of TRP is engaged. The -OH (s) peak from TRP (-COOH) at 6.79 ppm confirms the integration of TRP with the pure PU. The peak at 8.3 ppm (singlet) corresponds to the -NH peak due to urethane linkage in all the systems[173,174]. Notably, there are four different types of -NH (singlet) protons ranging from 8.30-9.93 ppm presents[175]. The -NH (-NHCONH-) moiety attached to urethane is at 8.3(t), while the moiety attached to TRP (d) appears at 9.7 ppm, and the biuret (o) moiety (-N-CO-NH-) appears at 9.92 ppm[176,177]. The (-NHCOC-) -NH(m) appears at 9.06(singlet)ppm, confirming the presence of the TRP and secondary >N-H of TRP are involved in the reaction, while in the other, only the primary linkage with urethane. Additionally, at 2.5 ppm (s, $–CH_2$ of TDI) is observed[178](the NMR of PU-TRP 6% is presented in **Figure 4.2.a)**.

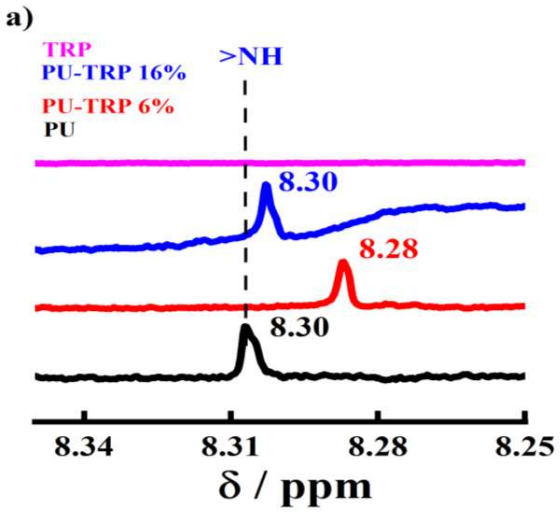

Figure 4.2: a) ^1H NMR for all the samples showing the tagging of TRP

The evidence supporting the grafting or chemical tagging of Polyurethane (PU) onto TRP is demonstrated through the FTIR absorbance peak at 1736 cm^{-1} (non-H-bonded)[129] assigned for urethane >CO (-$NHCOO^-$) in pure PU where the same peak shifted to 1728 cm^{-1} in PU-TRP 6% (low grafted PU) & 1709 cm^{-1} in PU-TRP 16% (high grafted). Since the graft copolymers display a hydrogen-bonded>CO this characteristic is very much prominent in pure PU, as confirmed by the H-bonded >CO peak at 1660 cm^{-1} [148,179]. However, the intensity of this peak significantly diminishes as the degree of substitution increases, suggesting limited intramolecular hydrogen bonding in the highly substituted graft copolymers as depicted in **Figure 4.2.1.b.**

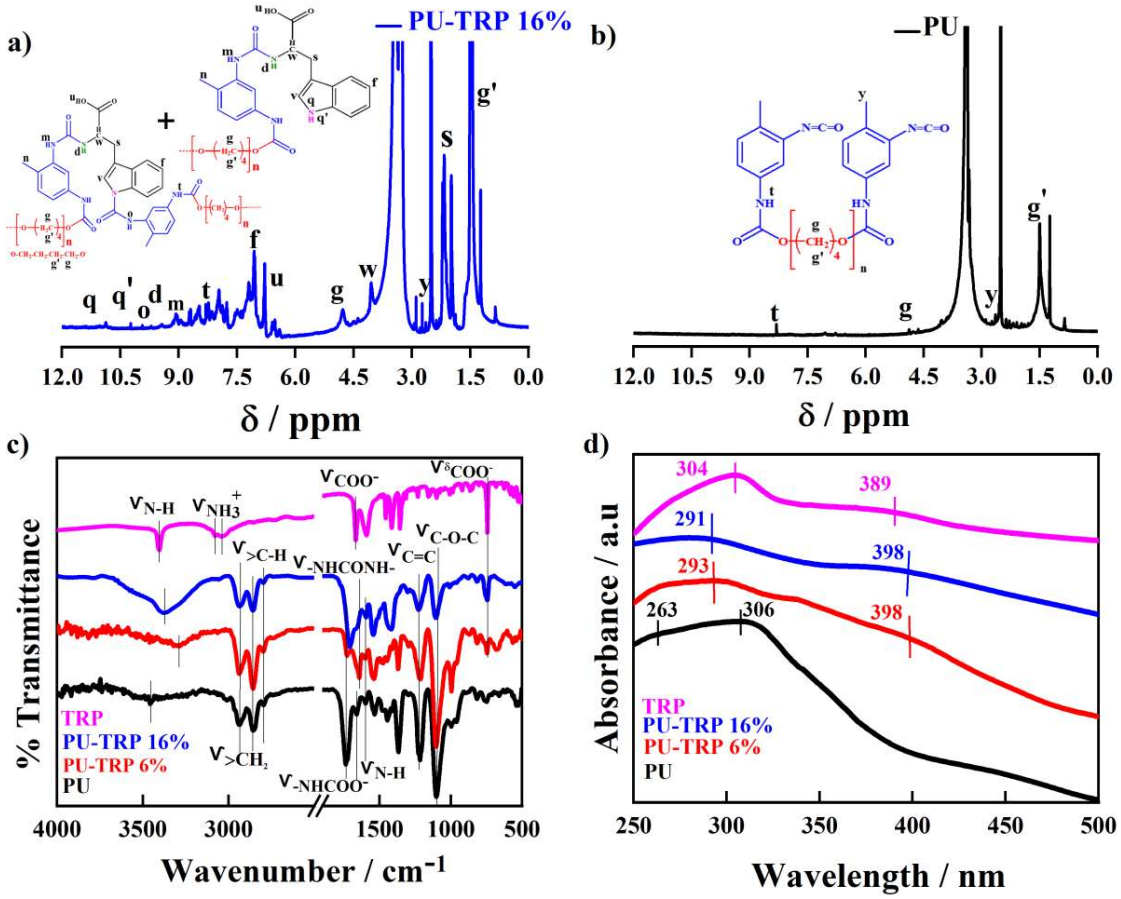

Figure 4.2.1: ^{1}H NMR of **a)** the highest grafted and **b)** pure PU, where the peaks are as labeled as "a" and "b" etc, **c)** FTIR spectra of all the specimens display shifts in peak positions resulting from interactions, **d)** UV–VIS spectra illustrate peak positions for the $\pi \rightarrow \pi^*$, $n \rightarrow \pi^*$ transition of the carbonyl peak and marked by vertical lines.

The stretching peak at 1660 cm^{-1} for COO^{-1} in TRP[180] and 1641 and 1649 cm^{-1} peaks for >CO (-NHCONH-) in both grafted copolymers confirm the tagging of TRP moiety in PU. Another moderately strong peak at (1597,1600, 1595) cm^{-1} shows the in-plane bending mode of >N-H in all the moieties[131] , and the existence of C=C bond, attributed to the benzene ring is indicated by a broad absorption peak centered around 1221 cm^{-1}[1131], whereas C-O-C stretching in the hard segment is evident at 1105 cm^{-1} [126]. A strong peak appears for all the grafted copolymers at around 744 cm^{-1} is a characteristic peak of TRP [181]. The peaks observed at 2934 and 2858 cm^{-1} are a result of anti-symmetrical and symmetrical stretching vibrations of -CH_2 unit present in both the pure PU and grafted one, as the degree of polymerization increases, there is a reduction in the peak intensity [131] and a small peak appears around 2795 cm^{-1} [182,183]. The broad spectral region around (3376,3288,3458) cm^{-1} corresponds to the >N-H stretching and shows similarity between the grafted PU with pure PU indicating excessive intermolecular hydrogen bonding in the grafted one [129]. Additionally, the >N-H in indole ring of TRP at 3403 cm^{-1} [181] disappears in the modified PU merely confirming both amine groups are involved in the polymerization reaction. Other than this the peak due to -NH_3^+ of TRP (in zwitter ion form two N-H peak appears one due to H-bonding and other due to non-bonding) shift to 3064 in PU-TRP 16% and 3057 in PU-TRP 6% from 3078 cm^{-1} [181]. The UV−Vis spectra for all samples were examined in the range of 250− 500 nm shown in **Figure 4.2.1.c**, pure PU displayed distinct absorption bands at 263 and 306 nm, corresponding to $\pi-\pi^*$ and $n-\pi^*$ transition, respectively. Notably, when

comparing UV−vis absorption peaks of grafted polymers, a consistent shift towards longer wavelengths is observed as we move to PU-TRP 16% (291 and 398 nm) and PU-TRP 6% (293 and 398 nm). This shift towards the red end of the spectrum (Bathochromic shift) can be attributed to the introduction of aromatic amino-acid into the system leading to extended conjugation[184,185].

4.2.2 Crystallinity and Structure in correlation with Morphological investigation and Thermal properties

X-ray diffraction (XRD) analysis was conducted to investigate the crystallinity of the samples utilized in this study (**Figure 4.2.2a**). The results indicated that none of the samples exhibited significant crystallinity, and therefore, no level of crystallinity was necessary to explain the structure and property differences among the samples. In all samples, a solitary diffuse peak was observed at approximately $2\theta=20^{\circ}$ [132,186]. Pure PU demonstrates a specific level of crystallinity, probably attributed to the crystalline nature of PTMG, which fails to integrate into the PU lattice post-polymerization [187,188]. PTMG crystallite peak is evident at around $2\theta=40^{\circ}$ [189]. The findings from these investigations suggest that the soft segment lacks the necessary length for crystallization and the asymmetry of the diisocyanate makes the formation of hard-segment crystallites unlikely. To confirm this deduction, two types of samples underwent XRD testing. Subsequently, a quenched sample underwent programmed annealing on a hot plate at 70℃ for XRD. Once again, only an amorphous peak was found (**Figure 4.2.2.1**). The above outcomes proposed that the hard segment (TRP) in PU-TRP does not exhibit remarkable crystallinity, potentially due to its relatively low content[190]. Since the crystallization impact of PTMG can be dismissed, the endothermic and exothermic peaks in DSC (**Figure 4.2.2c**) test might be linked to the association and dissociation of hard

segments[191,192]. Pure PU shows a smooth surface with no pore structures (**Figure 4.2.2b**). As the content of hard segments rises the material may go through phase separation, in which the hard and soft segments separate. The homogeneous structure may be disrupted by this phase separation, giving the illusion of increased granularity[193]. This microphase separation occurs due to the chain extender's ability to increase the hard segments' crystallinity. In contrast to the original smooth structure, this may result in a rougher, more porous texture.

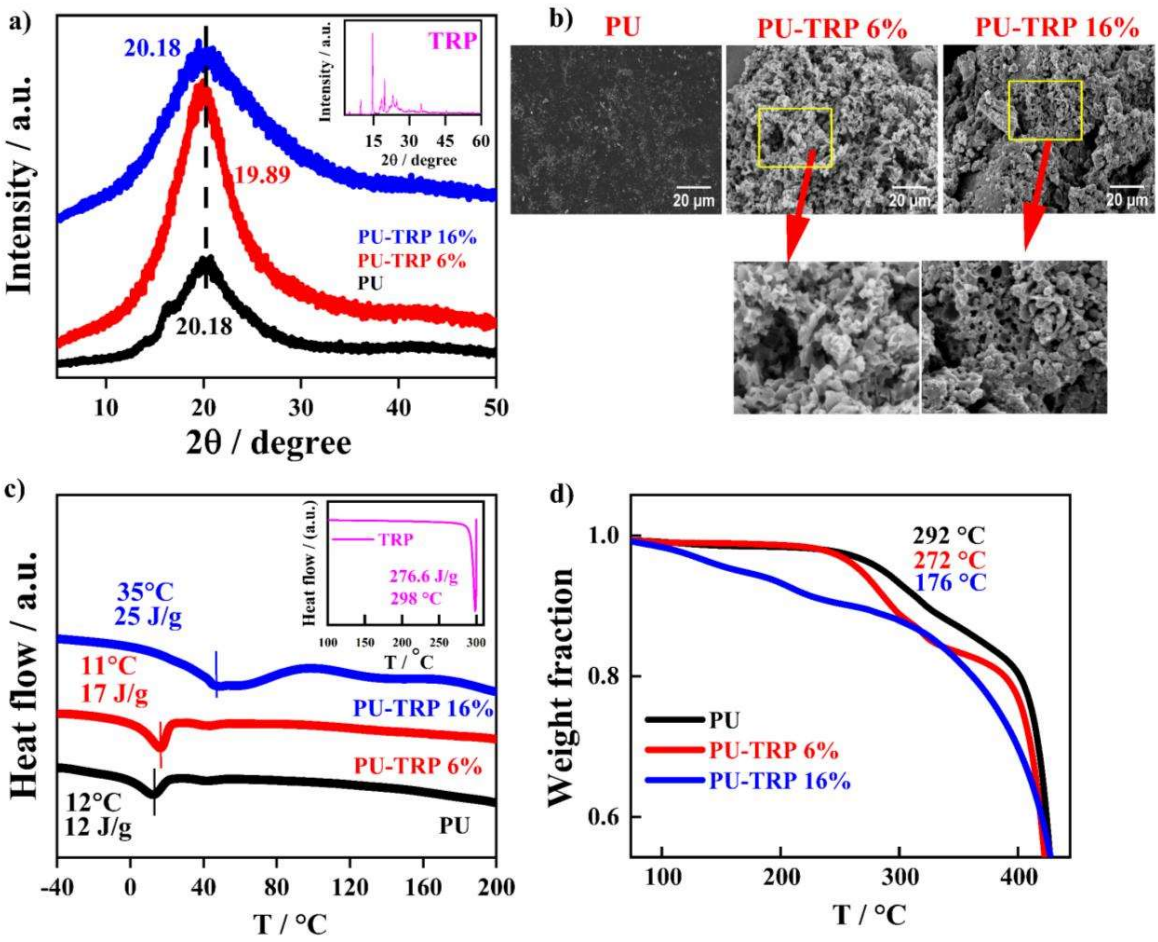

Figure 4.2.2: a) XRD patterns of all the samples, highlighting their crystallinity, b) SEM images showing the morphology of various PU samples, with zoomed images to show more clear visions, c) DSC thermograms of various PU samples are displayed, with melting temperatures and heat of fusions indicated in the corresponding color codes, d) Thermal stability (TGA thermograms) of all PU samples as measured through a thermogravimetric analyzer.

The microstructure may be impacted by the inclusion of a chain extender, which can raise the crosslink density in the polymer network[194]. A more porous shape of the material can result from cross-linking, which can produce microvoids or pores inside it.

The thermal characteristics of PU films were assessed using DSC to investigate micro-phase separation (**Figure 4.2.2c**) [195]. The observed trend in T_g across all specimens follows PU-TRP 16%> PU> PU-TRP 6%, representing a gradual increase in value from pure PU to the highest grafted one. However, the initial decrease in the case of the low-grafted sample is likely a result of enhanced interaction between the components, allowing overlap between individual components[196]. This variation is primarily attributed to differences in cross-link density. The heightened T_g in PU-TRP 16% is ascribed to a more significant extent of hydrogen bonding, resulting in a higher physical cross-link density. This increased density restricts the movement of PU chains. In case of the highest grafted PU with increased graft density, there is a subsequent rise in T_g, facilitating the crystallization of a larger number of PTMG units. This discrepancy is linked to a higher chemical cross-link density, aligning with findings from previous reports [197].

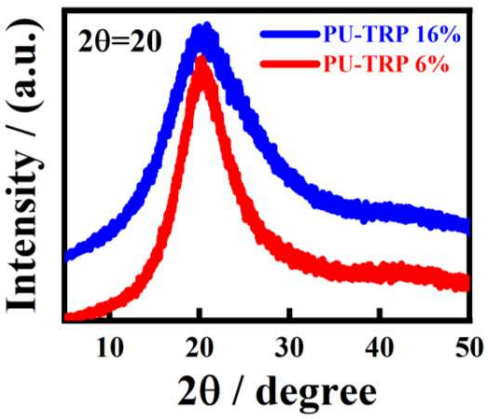

Figure 4.2.2.1: XRD patterns of all the samples, after annealing at room temperature

TGA (mass loss curve) was utilized to investigate the non-oxidative thermal degradation characteristics of various PU samples as depicted in **Figure 4.2.2.d**. The two-step degradation of PU in an inert atmosphere initiate at 320 ℃, extending to around 435℃, corresponding to the temperature at which 5% weight loss is observed in the sample. Notably, a three-stage degradation is evident in the case of lower grafted PU, whereas PU-Trp 16% displays multistep degradation (distinctly observed in DTA endotherm). The DTA signal highlights that the hard segments degrade at lower temperatures, while the soft segments at higher temperatures, reflecting their respective abundance within the overall PU chains. This phenomenon is likely attributed to the smaller size, greater quantity, and uniform distribution of the grafted segments compared to pure PU. The hard segment, consisting of urethane linkage, proves to be more susceptible to heat-induced degradation, with isolated crystallites degrading first exclusively from the hard segments, followed by scattered crystallites embedded in soft segments. The second step, associated with a secondary degradation process, exhibits a maximum rate of mass loss, indicating the degradation of the polyol unit (PTMG). This step yields more volatile material compared to the degradation of the urethane linkage[152,161,198].

4.2.3 Determining Critical Micelle Concentration from UV-VIS Spectroscopy

The concentration of materials above which micelles form is known as the critical micelle concentration or CMC. Optical density graph from UV-VIS spectroscopy **(Figure 4.2.3.1b.)** showed that all the modified polymers including TRP (due to its zwitter ion form)[199] exhibit two distinct CMCs, with one for **aggregation**[200] and another for **consolidation**, this likely suggests a more complex self-assembly process (Aggregation induced absorbance/AIA).

This may induce changes in the molecular structure (e.g., folding, stacking), leading to new electronic transitions or enhanced absorption at specific wavelengths. The absorbance values (PU-TRP 16%) show a sudden shift from sharp to broad on increasing concentration, when it reaches 400 µg/ml (for pure TRP and PU-TRP 6% it is 150 µg/ml and 1000 µg/ml respectively, the higher value of concentration in the latter case probably because of the lower tagging of TRP) the broadness becomes more visible as seen in **Figure 4.2.3.1a. (**the change in absorbance values on increasing concentration for PU-TRP 6% and TRP is shown in **Figure 4.2.3.2 a and b).** The CMC values are calculated by plotting optical density vs log concentration at wavelength 266 nm for all the samples at a variable concentration (**Figure 4.2.3.1b.**). The CMC values are given in tabulated format below in **Table 4.2.3** for all the test samples.

Table 4.2.3: CMC values of all the samples

Intersection points from the graph along with Concentration (µg/ml)		
TRP	**PU-TRP 6%**	**PU-TRP 16%**
x=1.33 (0.12) **y=1.66**	**x=1.88 (0.27)** **y=1.01**	**x=1.56 (0.19)** **y=0.78**
x=2.19 (0.34) **y=4.66**	**x=2.41 (0.38)** **y=2.88**	**x=2.30 (0.36)** **y=3.09**

The absorption peak is moving to longer wavelength that happens due to increased conjugation or stacking interactions in the aggregated state, where the first CMC marks

probably because of the formation of small micelles and the second marks the growth or rearrangement into more complex vesicles-like structures. The ionization of amino-acid residues in the PU-TRP segment[201] could be another reason for the increase in the second CMC (from 0.27 to 0.38 µg/ml in PU-TRP 6% and in PU-TRP 16% 0.19 to 0.36 µg/ml).

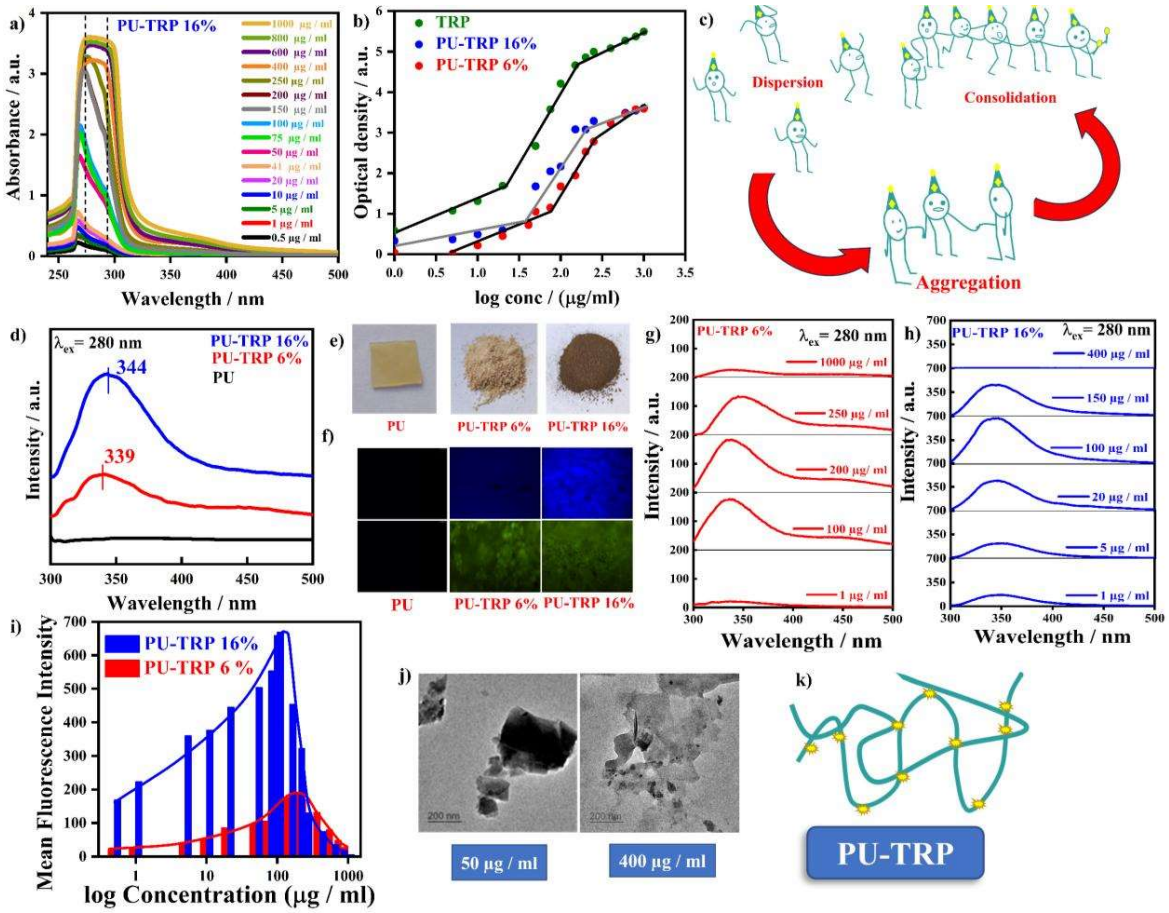

Figure 4.2.3.1: a) The variations of absorbance on increasing concentration for PU-TRP 16%, b) optical density vs concentration plot for all the samples showing CMC at two intersection points, c) Schematic illustration showing the mechanism of AIA, d) Fluorescence emission spectra of all the test samples, e) Images of samples taken by phone camera, f) The fluorescence images of all the samples, g) and h) Concentration driven fluorescence spectra of both PU-TRP 6% and PU-TRP 16% respectively, i) Mean fluorescence spectra of both the modified polymers, j) TEM images of PU-TRP 16% at 50 and 400 µg/ml concentration showing aggregation and consolidation, k) Schematic showing the structure of PU-TRP.

This may be attributed to the deprotonation of a portion of the -COOH groups of tryptophan in PU-TRP section, which increased the molecular polarity and required more driving energy for micellization to offset the increased electrostatic repulsive force. Molecules with more hydrophilic character are less likely to come together to form micelles, as micelle formation is often driven by the need to shield hydrophobic parts of molecules from the aqueous environment. The fluorescence spectroscopy of pure PU (in DMF) exhibits no peak as shown in **Figure 4.2.3.1d**. However, after functionalization with TRP, it reveals a λ_{max} at 344 nm[202] for the highest grafted one and 339 nm for the lowest grafted polymer (λ_{EX} =280).

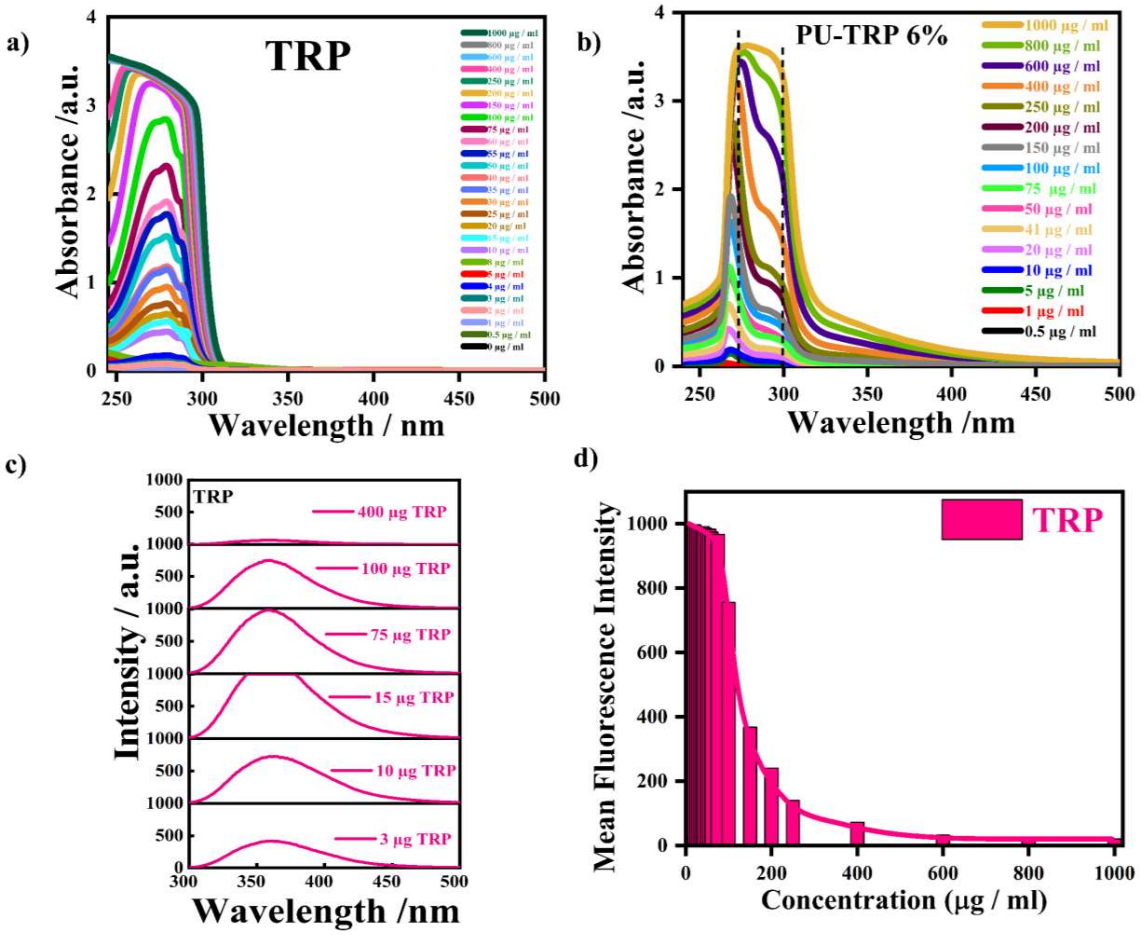

Figure 4.2.3.2: shows aggregation-induced absorbance for a)TRP, and b)PU-TRP 6%, c) fluorescence quenching for TRP, d) MFI of TRP

The modified PUs fluoresces both blue and green, as seen in the microscope photos (**Figure 4.2.3.1f**). These colors are most likely caused by TRP's intrinsic fluorescent[202,203] characteristics. The green fluorescence may result from energy transfer (Trp is the fluorophore donor and the polymer matrix is the acceptor) within the polymer matrix, indicating the occurrence of the FRET because of the large complex structure. The blue fluorescence is typically caused by the tryptophan itself. A visual representation of the polymer structure is given in the schematic diagram **Figure 4.2.3.1k**. Additionally, we can observe the fluorescence quenching in **Figure 4.2.3.1g** and **h**, which further supports the AIF or aggregation-induced fluorescence phenomenon. As concentration increases, CMC formation takes place, changing the molecular conformation and causing the fluorescence to be quenched. The maximum fluorescence for PU-TRP 16% is 200 µg/ml, and for PU-TRP 6%, it is 100 µg/ml {the maximum fluorescence of TRP is 75 µg/ml, as shown in **Figure 4.2.3.2) c**}. The MFI values of PU-TRP 6% and 16% are also given in **Figure 4.2.3.1i** supporting the fluorescence quenching as well as the AIF[202,203] phenomenon which is also visible in pure TRP. The micellization is also confirmed by the Tem images (**Figure 4.2.3.1j**) of PU-TRP16% the initial aggregation induced small micelle formation (50µg/ml) and from that larger structure formation (400µg/ml) due to consolidation.

4.2.4 Sustained reléase of drug using varying PU structure

The cumulative release of PTX from all systems in a PBS solution over time is depicted in **Figure 4.2.4a**. A similar amount of drug (5 wt % relative to the polymer weight) was incorporated into the PUs. In 24 hours, PU releases 8% of the embedded drug, PU-TRP 16% releases 72%, and PU-TRP 6% releases 34%. The release pattern of PTX in PBS buffer indicates a steady and sustained release from all systems, likely due to stronger hydrogen-

bonding interactions between the drug and the polymer, as confirmed through molecular docking experiments shown in **Figure 4.2.4d**, with corresponding values in **Table 4.2.4.2**. Kinetic parameters derived from the Higuchi model[204] indicate $r^2 \sim 0.97$ for the highest grafted system, suggesting a non-Fickian release mode (**Figure 4.2.4b** illustrates the drug release mechanism via various kinetic models, with values in **Table 4.2.4.1**). For PU and PU-TRP 6%, r^2 values are ~0.92 and ~0.97, respectively, following the KP model.

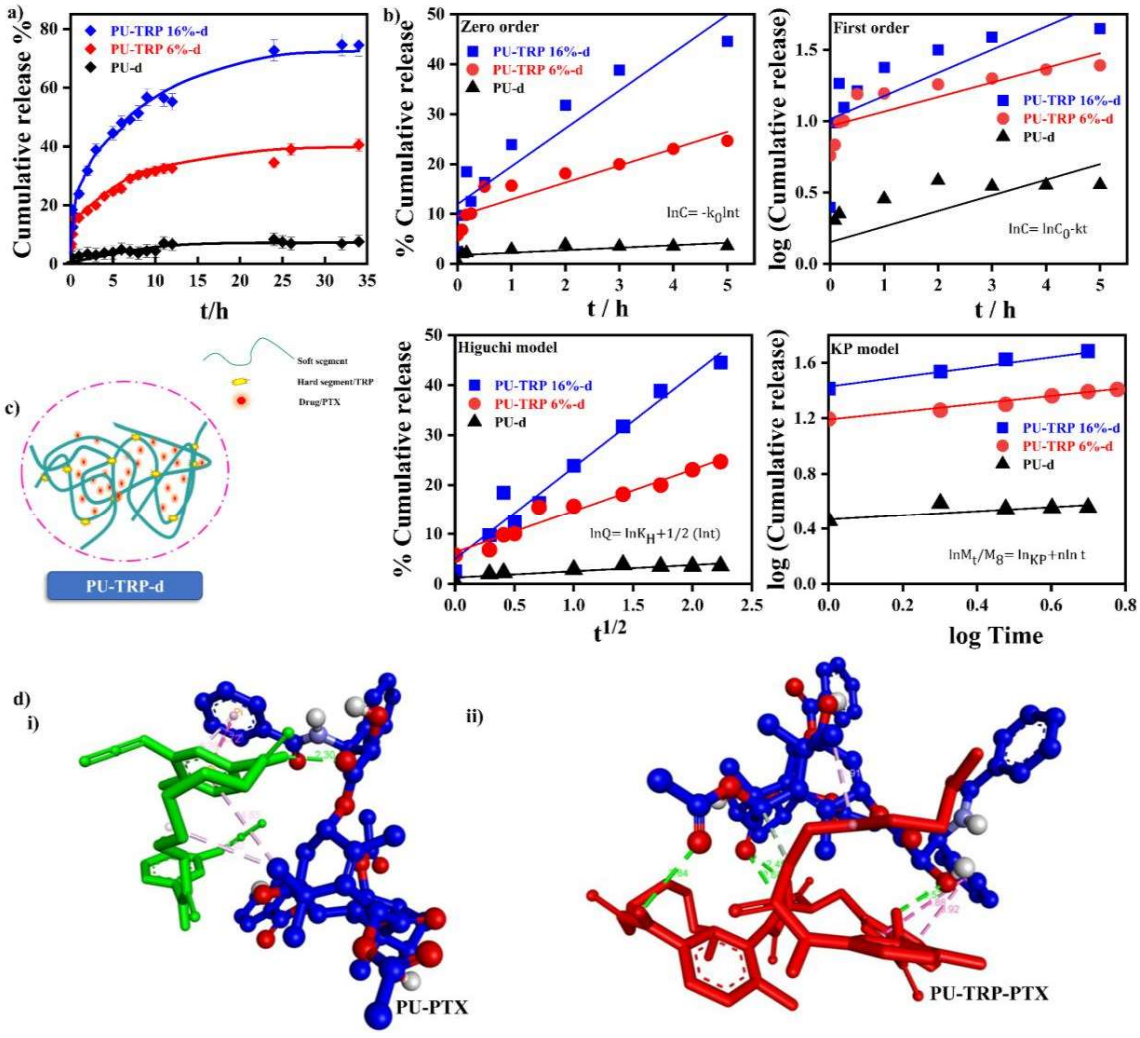

Figure 4.2.4: a) Cumulative drug release from the specimens showing sustained drug release profile from the polymers, b) Drug release profiles of all of the specimens, c) Schematic model showing the architecture of different PU-TRP loaded with a drug that causes sustained

release, d) Molecular docking images showing drug-polymer interaction i) PU and ii) PU-TRP.

The slower release from PU can be explained by the molecular docking interactions which report that paclitaxel exhibited binding affinities to all grafted systems, with binding energies of -4.4 (PU) and -4.5 (PU-TRP 16% kcal/mol)[205]. The highest grafted polymer interacts with PTX residues through various interactions, such as (-NH-(primary)-TRP, -CO-PTX), (-NH-TDI, -OH-PTX), and others like (-CH2-PTMG, -CH-PTX), (-Ph-TRP, -Ph-PTX), and (-Indole-TRP, -Ph-PTX)[206].

Table 4.2.4.1 Parameters of drug release profiles using various PUs

Polymers	Zero-order	First order	Higuchi model	KP model
PU	Slope =0.46±0.16 Intercept=1.8±0.43 r^2=0.56	Slope = 0.1±0.06 Intercept=0.16±0.15 r^2 =0.37	Slope =1.22±0.27 Intercept=1.36±0.37 r^2 =0.77	Slope =0.15±0.02 Intercept=0.47±0.01 r^2 = 0.92
PU-TRP 6%	Slope =3.4±0.48 Intercept =9.5±1.38 r^2 =0.86	Slope =0.1±0.02 Intercept=0.97±0.05 r^2 = 0.71	Slope =0.1±0.02 Intercept=0.97±0.05 r^2 = 0.71	Slope = 0.28±0.01 Intercept=1.2±0.01 r^2=0.97

PU-TRP 16%	Slope=7.58±1.14 Intercept =11.9±2.38 r^2 =0.86	Slope =0.16±0.06 Intercept=1.02±0.12 r^2 =0.53	Slope =18.5±1.3 Intercept=5.02±1.5 r^2 = 0.97	Slope=0.4±0.05 Intercept=1.4±0.03 r^2 = 0.91

Other potential interactions between pure PU and paclitaxel are also shown in **Figure 4.2.4d(i)**, with the binding energies and interaction values listed in **Table 4.2.4.2**.

Table 4.2.4.2: Molecular docking values in Tabular form

Ligand-receptor complex compound	**Docking score (kcal/mol)**	**Type of bonds**	**Bond distance (Å) & interacting residues**
PU-PTX	-4.4	1 Hydrogen bond 1 Π-Π 3 Π-alkyl	2.30 (-CONH-PP, -COO-PTX) 3.72 (-Ph-TDI, -Ph-PTX) 4.02(-CH_2-PTMG, -CH_3-PTX); 4.26 (-CH_3-TDI, -Ph-PTX); 4.85 (-Ph-TDI, -CH_3-PTX);
(PU-TRP 16%)-PTX	-4.5	4 Hydrogen bond	2.45 (-NH (primary)-TRP, -CO-PTX); 2.57(-NH-TDI, -OH-

		1 carbon-hydrogen 1 alkyl-alkyl 2 Π-Π	PTX); 2.68 (-NH-TDI, -CO-PTX); 2.84(-NH-TDI, -CO-PTX) 3.45 (-CH_2-PTMG, -CH-PTX) 3.91 (-CH_2-PTMG, -CH_3-PTX) 3.92 (-Ph-TRP, -Ph-PTX); 4.88 (-Indole-TRP, -Ph-PTX)

This enhances the stability of the drug and polymer matrix complex through strong molecular interactions, such as hydrogen bonding and van der Waals forces, "trapping" the drug and preventing its degradation in biological conditions that can enhance targeted delivery and increase bioavailability. However, the drug may still be released rapidly if the polymer matrix is highly permeable, which could be the case due to the hydrophilic amino acid TRP. In pure PU, hydrophobicity primarily reduces drug release, whereas, in modified PU, TRP increases the structural rigidity as well as the number of interactions with the drug, but these factors are balanced by the hydrophilicity speeds, making PU-TRP 16% the most effective system among the three. Adding a hydrophilic hard segment increases the water uptake rate[207] in PU, influencing the drug release rate by increasing the network porosity of PU that allows the hydration and water absorption, creating water channels within the polymer network that facilitate drug diffusion and release[208].

4.2.5 Biocompatibility and *in-vitro* treatment efficacy

The biocompatibility of drug carriers has to be ensured for them to be used successfully in biomedical applications, thus ensuring that therapeutic treatments are safer, more effective, and reliable. In this research, biocompatibility was evaluated by studying the adhesion of cells using phase-contrast imaging of 3T3 and SiHA cells. The results showed improved cell adhesion to the modified PU (TRP grafted ones 6 and 16%) structures, as evidenced by the well-spread morphology of the cells (**Figure 4.2.5.1 a** and **b** for SiHA and 3T3 cells, respectively)[209–213]. The 3T3 cell images were captured at 20× magnification, while the SiHA cell images were captured at 40× magnification to better visualize cell morphology, as 3T3 cells range from 50–100 μm in length, while SiHA cells are 20–50 μm long. However, the cell length is different for different material beds[207]. The OD values were 105% for 3T3 and 132% for SiHA cells after 24 hours (PU-TRP 16%), which proved the better adhesion of the PU-TRP based material on cancer cells than the healthy muscle cells (**Figure 4.2.5 c, d**). The OD value of the PU-TRP16%-SiHA system was much higher, suggesting that TRP-based PU is more effective for the treatment of cancer. Improved adhesion to cancer cells may make targeted delivery of anticancer drugs more efficient by reducing off-target effects and concentrating therapeutic agents at the site of the tumor, thus making the treatment more effective. Highly permeable blood vessels have been linked to cancer cells due to enhanced permeability and retention effects attributed to rapid and disorganized angiogenesis that happens in a tumor[214]. Consequently, gaps between endothelial cells lead to the easy passage of macromolecules into a tumor when compared to normal tissues. As a result, the EPR effect[72] is more prominent in *in-vitro* experiments involving cancer cells. The present study serves as a proof-of-concept, demonstrating the drug-delivery potential of the newly developed TRP-based PU. Moreover, the biological responses of the samples were evaluated

using MTT assays on 3T3 and SiHA cell lines over three consecutive days, with concentrations ranging from 20 to 100 µg/mL. The results demonstrated that modified PU-TRP16% showed better biocompatibility than pure PU, with corresponding OD values shown in **Figure 4.2.5.2a** for SiHA and **b** for 3T3, aligning with literature reports[207,215].

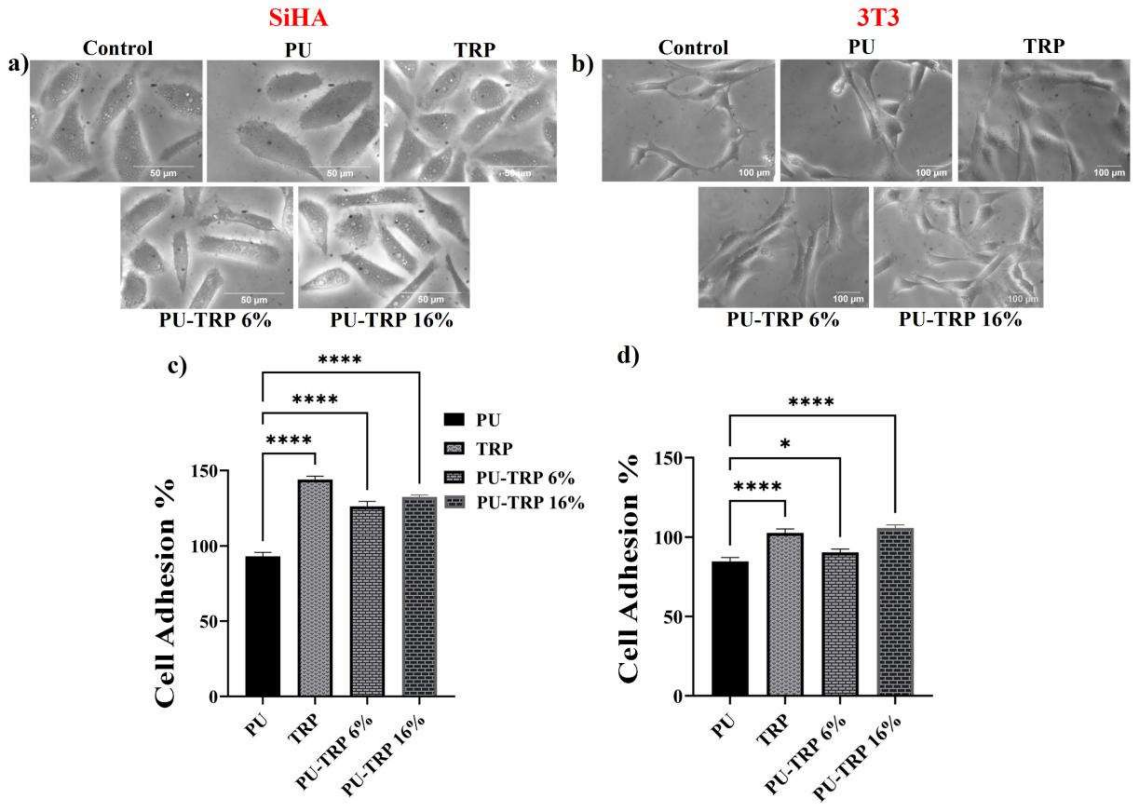

Figure 4.2.5.1: Biological responses of all the polymers assessed through cellular studies, a) Morphology of 3T3 cells grown on polymer surfaces as captured through microscopy on a gray filter after 1 day of sample proliferation (cell adhesion magnification: 20×); b) Morphology of SiHA cells grown on polymer surfaces as captured using microscope on a gray filter after 1 day of sample proliferation (cell adhesion magnification: 40×); c) Evaluation of cell adhesion using optical density profile data for adhered 3T3 cells across the sample bed; and d) Evaluation of cell adhesion using optical density profile data for adhered SiHA cells across the sample bed.

PU-TRP 16% maintained over 89% cell viability even at higher concentrations (100 µg/mL) after three days in 3T3 cell line whereas, for SiHA at this concentration, the OD value on

day 1 was 117% although it dropped to 72% on day 3 (probably because it contains aromatic systems of PU as more consumption of material by cancer cells, to meet up their heightened metabolic rate). These results indicate that TRP-modified PU (16%) preferentially interacts with cancer cells and is safer to use in the biomedical field. However, additional *in-vitro*

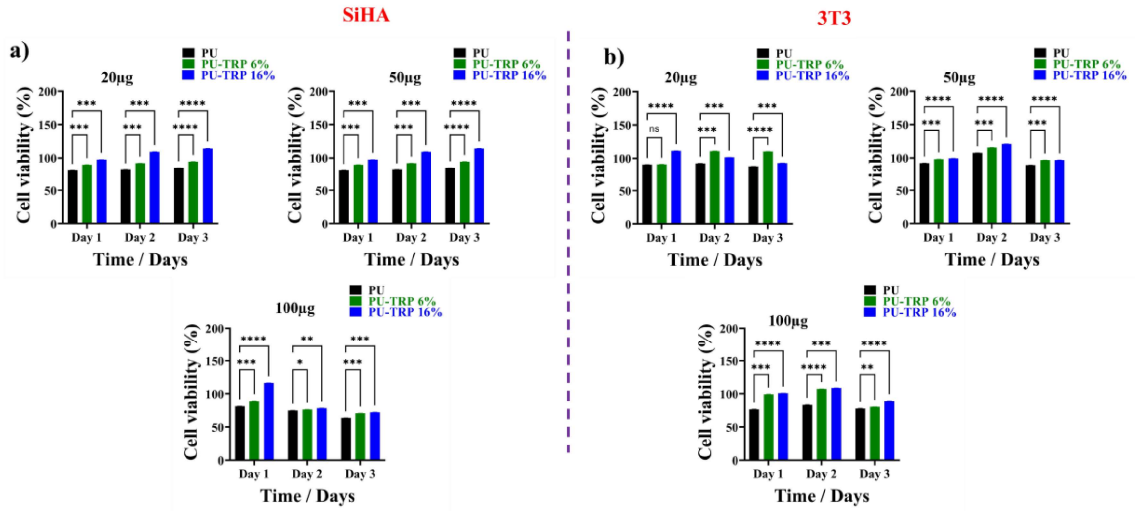

Figure 4.2.5.2: *In-vitro* cytotoxicity of all polymers on a) SiHA and b) 3T3 cells at a 3-day span assessed using the MTT assay at a concentration of 20 µg/ml, 50 µg/ml, 100 µg/ml.

studies are required to evaluate the differences in cell-killing efficacy between free PTX and drug-loaded polymers. For pure drug, treatments, cell viability generally increased over time, suggesting a reduction in cell mortality. However, a slight increase in cell death was observed on day 1 (**Figure 4.2.5.3a** for SiHA cells, with the corresponding AO/PI image for 20 µg/mL shown in **b**), likely due to the immediate exposure to the cellular media. In contrast, for the 3T3 cell line, cell death increased over time (**Figure 4.2.5.3c** for 3T3 cells, with the corresponding AO/PI image at 20 µg/mL in **d**). Both cancer and normal cells share similar target molecules (such as enzymes or receptors), which can lead to unintended effects on normal cells. This is where the selective killing of up to 14% of SiHA cells after 3 days of

treatment, while maintaining 95% cell viability in 3T3 cells at the same dosage, comes into action by the vehicle PU-TRP16% (20 µg/mL). Malignant cells produce high levels of matrix metalloproteinases, enzymes that digest the extracellular matrix (ECM), making it possible for larger molecules to cross the cells more easily owing to compromised membrane permeability. Cancer cells take in extracellular fluids, nutrients, and protein building blocks like TRP, an α-amino acid, to meet their high metabolic needs when subjected to hypoxia or an acidic environment through endocytosis[207]. The acidic environment can enhance polymer swelling, prodrug hydrolysis, promoting faster drug release in tumor regions, pH (~2–4) compared to normal cells. While SiHa cancer cells exhibit rapid paclitaxel-induced cytotoxicity due to high proliferation rates and mitotic sensitivity, 3T3 fibroblasts demonstrate delayed toxicity, likely resulting from cumulative drug exposure and less efficient stress adaptation mechanisms. Additionally, the free drug lacks selectivity and diffuses indiscriminately into both cell types, contributing to delayed but significant cytotoxic effects in normal cells by Day 3. This underscores the importance of polymer-based delivery systems for selective and temporally controlled drug release, and helpful in the development of sophisticated therapies for cancer.

To understand the mechanism behind cell killing or drug-induced apoptosis by drug-loaded vehicles or pure drugs, both cell types were analyzed using fluorescent imaging after AO and PI staining. This dual-staining technique after AO and PI staining. This dual-staining technique differentiates between normal and apoptotic cells by assessing membrane permeability. AO can penetrate the cell membrane, bind to DNA, and emit, while PI emits red fluorescence. Dead cells, which allow both AO and PI to enter, appear red, while healthy

cells, which only allow AO to enter, appear green. Cells with an orange-yellow hue after staining indicate apoptosis or early necrosis, with red fluorescence indicating compromised

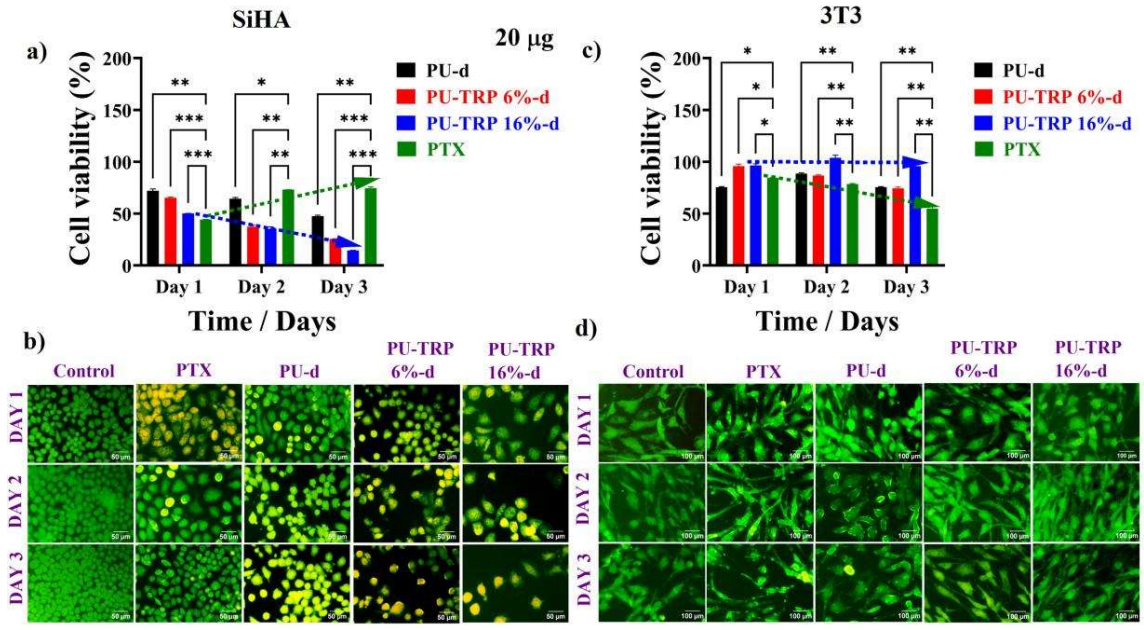

Figure 4.2.5.3: a) *In-vitro* cytotoxicity of pure drug and, drug-loaded PUs on SiHA cells at various time intervals assessed using the MTT assay at a concentration of 20 µg/ml, b) Fluorescence images of SiHA cells after AO/EB staining, treated with pure drug and drug-loaded polymers at a concentration of 20 µg/ml, captured at 20× magnification, c) *In-vitro* cytotoxicity of pure drug and drug-loaded PUs on 3T3 cells at different time intervals evaluated using the MTT assay at a concentration of 20 µg/ml; and d) fluorescence images of 3T3 cells after AO/EB staining, treated with pure drug and drug-loaded polymers at a concentration of 20 µg/ml, captured at 20× magnification.

membrane integrity[196]. Normal healthy cells show green fluorescence. The SiHA cell line treated with the drug-loaded PU-TRP16% shows reduced cell density and predominantly apoptotic cells, while 3T3 cells remain viable after 3 days, consistent with the MTT assay results. Notably, the highest tumor cell killing efficiency was observed with PTX-embedded PU-TRP16%, while its normal cell killing rate was the lowest, demonstrating its greater efficacy in targeted tumor treatment compared to pure drug or drug-loaded PU. While both

PU-TRP-d systems contain the same amount of drug (5% w/w) and show different therapeutic efficacy, the difference in TRP tagging percentages may lead to variations in polymer physicochemical properties that can influence tumor targeting and drug release behavior. The hydrophilic/hydrophobic balance of the polyurethane matrix can modulate drug release kinetics and polymer–cell interaction. As we can see from the release profile (in Figure 4.2.4a) in **section 4.2.4**, PU-TRP 6%-d releases 34% and PU-TRP16%-d releases 72% in 24 hours. So, changes in TRP tagging could influence surface properties (e.g., charge, hydrophilicity), potentially affecting cellular uptake or biodistribution. This also highlights the superior role of TRP as a chain extender in designing a more effective drug delivery vehicle. Though cell cycle analysis is crucial for assessing the effectiveness of mitotic inhibitors, such as paclitaxel, because it sheds light on the drug's mode of action. Our study primarily focused on cell viability assays to ascertain the net cytotoxic impact of paclitaxel on SiHA and 3T3 cells. This approach was fashioned to set the stage for drug efficacy before exploring further into more mechanistic-specific details. The lack of cell cycle distribution information limits the intensity of our analysis, particularly for the observed extended G2/M arrest in SiHA cells. This limitation makes it clear that although cell cycle analysis would be useful in yielding further mechanistic information, but it is beyond the scope of our work.

4.2.6 Cellular uptake in healthy cells along with fluorescence imaging in cancer Cell

Drug release, cellular studies, as well as MFI confirmed that PU-TRP 16% is best among the three of them, so we performed cellular uptake in healthy cells (**Figure 4.2.6a**) with this one system. The study confirmed the fact established by the MTT assay that in 3T3 the material fluorescence is maximum at 24 hour and after that, it starts to be excreted out from the cells

causing no toxicity (even at 100 µg/ml concentration, compared to cancer cells where viability drops to 72% at day 3. This indicates that healthy cells take up the material temporarily and then presumably clear it through processes like exocytosis or efflux transporters. This clearance is fast and is accompanied by minimal toxicity, even at high levels (100 µg/mL), and is in accordance with normal cell physiology, where nonspecific uptake is often followed by efficient clearance, leading to a shorter fluorescence duration. Along with that, we have captured the fluorescence images (**Figure 4.2.6b**) of the material inside the cell at the same concentration in SiHA cells supports the fact that the material shows fluorescence inside the cells as well. In cancer cells, the material shows maximum fluorescence on the 3rd day; it can easily penetrate due to angiogenesis, and the penetration is sustained, so the drug-loaded matrix will also show sustained release.

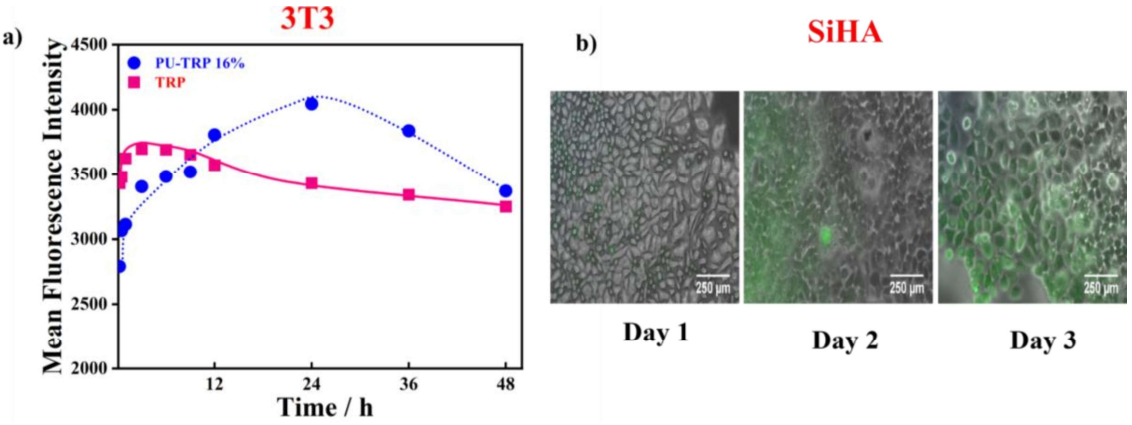

Figure 4.2.6: a) Cellular uptake inside the healthy cells up to 48 hr., b) Fluorescence images of sample inside the cell.

This aligns with well-documented tumor pathophysiology, where haphazard angiogenesis and impaired lymphatic drainage increase the Enhanced Permeability and Retention (EPR) effect to facilitate deeper and longer-lasting material deposits. Consequently, SiHA cell

viability reduced to 72% on day 3 (Figure 4.2.5.2a), indicating successful internalization and therapeutic action. Fluorescence microscopy (Figure 4.2.6b) also verifies the intracellular site of the material in SiHA cells, confirming its use in long-term retention and possible therapeutic action[216,217].

These findings demonstrate that the material shows behavior typical of tumor-targeted systems, such as increased uptake, extended retention, and improved cytotoxicity in cancer cells. Above all, the fact proved that the material can be a good option for diagnosis and therapy as well.

4.2.7 *In-vivo* release and gelation study to check localized treatment efficacy

Encouraged by this sustained release *in-vitro* and by observing the good cell mortality rate in the cellular study, an *in-vivo* experiment was performed to evaluate the therapeutic performance of the PU-TRP 16% system in an animal model. The gelation study is done by subcutaneous injection of drug-loaded polymer (PU-TRP16%) entrapped in MC-gel (**Figure 4.2.7.1**), and images of mice were captured before and after the subcutaneous injection. The bulge formation immediately after the injection confirms the solidification of the material below the skin layer. The histopathology (H& E staining), as well as TNFα images[196] (**Figure 4.2.7.2a**), staining in normal vs Gel skin (the schematic diagram of MC-gel-PU-TRP16%-d is given in **Figure 4.2.7.2b)** confirmed that the morphology remained intact in both normal and injected skin sections, as well as no sign of inflammation was visible in the skin section post-injection.

In this investigation, the high-grafted material was administered through both intraperitoneal

Figure 4.2.7.1: Gelation study via subcutaneous injection of drug-loaded polymer (PU-TRP16%) entrapped in MC-gel, and images of mice were captured before and after the subcutaneous injection.

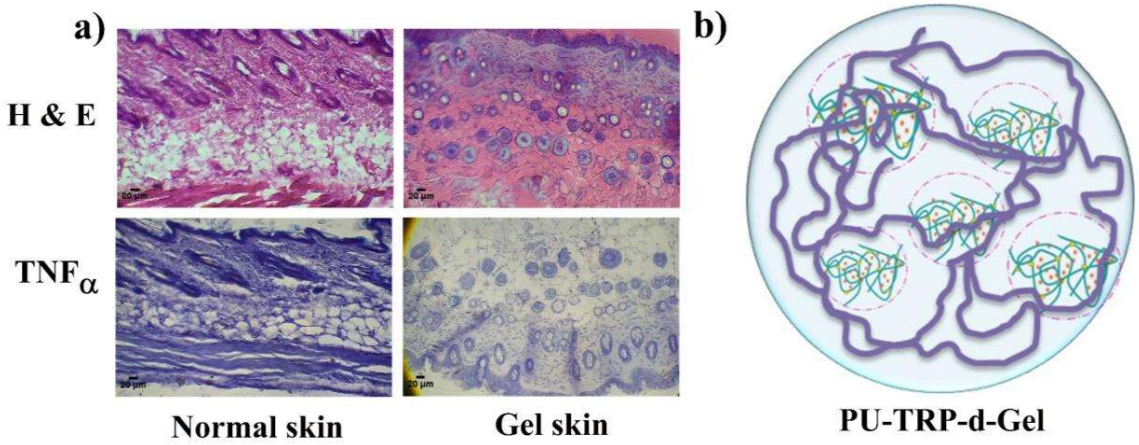

Figure 4.2.7.2: a) H&E and TNFα of normal vs gel skin, to check inflammation or any possible change, b) schematic diagram representing MC-gel-PU-TRP 16%-d

(IP) and intravenous (IV) routes in the animal model.

In the IV mode of administration, the pure drug shows a rapid release, peaking within a minute and then rapidly declining, which often necessitates a significantly higher dose. In contrast, our system reaches its peak concentration at around 6 hours, maintaining the minimum effective concentration (MEC), which helps sustain drug levels within the therapeutic window.

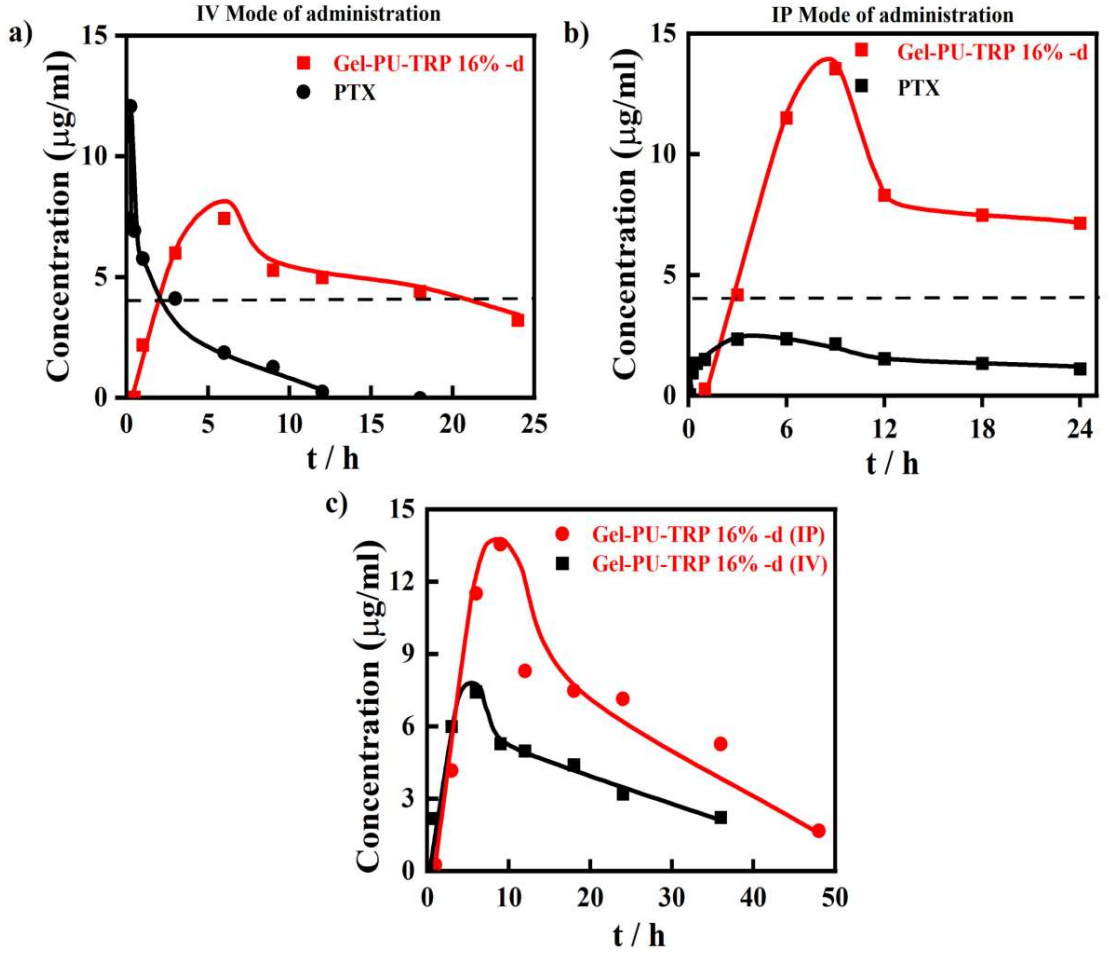

Figure 4.2.7.3: *In-vivo* release kinetics of MC-gel loaded drug-polymer matrix and pure drug in both modes a) IV and IP mode, and their comparison is given in c).

In the IP mode of administration, the pure drug, although shows sustained release but its

concentration failed to reach the minimum effective concentration (MEC), whereas the MC-gel-PU-TRP16% formulation is capable of showing sustained release within the therapeutic window and reaches maximum at 9 hours (**Table 4.2.7.4**).

Table 4.2.7.4: The quantitative time vs concentration data at different time intervals in both IV and IP mode

Time (h)	**IV Concentration (µg/mL)**	**IP Concentration (µg/mL)**
5 min	0.0121	0.2707
10 min	0.01445	0.85028
15 min	0.48596	0.88523
30 min	0.68677	0.9522
1	2.1793	2.27139
3	5.99045	4.16832
6	7.42248	11.50277
9	5.27485	13.5464
12	4.97462	8.29884
18	4.3954	7.47568
24	3.19586	7.13634
36	2.22054	5.25879
48	1.22836	1.66172

Comparative studies between the IV and IP modes have shown that the MC-gel-PU-TRP16%

formulation is capable of showing sustained release without causing inflammatory responses[196] in the skin, as seen by the subcutaneous injection test. This formulation is likely to be the most effective for localized treatment, ensuring enhancement of drug bioavailability along with selective targeting of the cancer cells and support of diagnostic purposes. The *in-vivo* release kinetics (**Figure 4.2.7.3**) have also supported the application of the material in real world.

4.3 Conclusion

Tryptophan (TRP)-based polyurethane (PU) was synthesized using TDI and PTMG as the hard and soft segments, respectively. This resulted in the formation of a PU having fluorescence-responsive properties along with improved biocompatibility and bioavailability. NMR, FTIR, and UV studies revealed the successful incorporation of TRP as a chain extender in the PU structure without affecting the viability of SiHA (tumor) cells and 3T3 (normal muscle) cells. Complementing pure polyurethane, TRP-modified PU shows enhanced hydrophilicity as well as better drug-entrapping characteristics, which helps to shield the drug in a biological system. It has shown to show 72% drug release after 24 hours against just 8% of the pure PU. Cellular assays indicate that the TRP-modified PU has better adhesion to cancer cells at OD values of 132% on SiHA cells and 105% on 3T3 cells, signifying a huge potential in selectively targeting tumor cells for treatment. The modified PU selectively kills up to 14% of SiHA cells, while retaining 95% of 3T3 cell viability at a concentration of 20 µg/ml. The drug release from the carrier is sustained and controlled over three days, thus reducing the frequency of drug administration. In addition to its drug delivery capability, TRP-modified PU has intrinsic fluorescence properties that make it applicable for diagnostic purposes. *In-vivo* experiments have confirmed its potential as an

effective candidate for localized tumor treatment with enhanced drug bioavailability at the target site. Future studies will aim to build on these findings by incorporating focal adhesion analysis using vinculin immunostaining. This approach will allow us to directly observe and quantify FA formation, offering additional insight into the mechanisms of cell attachment and spreading on various polymeric substrates.

We can conclude in the end, that TRP-modified PU (16%) has an extended release of drugs, good biocompatibility, and diagnostic capability, making it a suitable material for real applications.